

Choose What to Observe: Task-Aware Semantic-Geometric Representations for Visuomotor Policy

Haoran Ding¹, Liang Ma¹, Yaxun Yang¹, Wen Yang¹, Tianyu Liu¹, Anqing Duan¹, Xiaodan Liang¹,
Dezhen Song¹, Ivan Laptev¹, Yoshihiko Nakamura¹

Abstract—Visuomotor policies learned from demonstrations often overfit to nuisance visual factors in raw RGB observations, resulting in brittle behavior under appearance shifts such as background changes and object recoloring. We propose a task-aware observation interface that canonicalizes visual input into a shared representation, improving robustness to out-of-distribution (OOD) appearance changes without modifying or fine-tuning the policy. Given an RGB image and an open-vocabulary specification of task-relevant entities, we use SAM3 to segment the target object and robot/gripper. We construct an L0 observation by repainting segmented entities with predefined semantic colors on a constant background. For tasks requiring stronger geometric cues, we further inject monocular depth from Depth Anything 3 into the segmented regions via depth-guided overwrite, yielding a unified semantic–geometric observation (L1) that remains a standard 3-channel, image-like input. We evaluate on RoboMimic (Lift), ManiSkill YCB grasping under clutter, four RL Bench tasks under controlled appearance shifts, and two real-world Franka tasks (ReachX and CloseCabinet). Across benchmarks and policy backbones (Flow Matching Policy and SmolVLA), our interface preserves in-distribution performance while substantially improving robustness under OOD visual shifts.

I. INTRODUCTION

Learning visuomotor policies from demonstrations has enabled impressive manipulation behaviors [1], [2], [3]. However, these policies often remain brittle when deployed outside the training visual context [4], [5]. In particular, task-irrelevant appearance changes—such as tabletop color shifts, background clutter, or object recoloring—can induce severe performance drops even when task semantics and dynamics remain unchanged.

Recent progress has primarily focused on scaling model capacity, including generative policies (diffusion/flow) [1], [6], [7] and vision–language(-action) systems [3], [8], [9], [10]. While these approaches improve capability and task diversity, robustness to visual distribution shifts is typically addressed through data augmentation, broader pretraining, or additional sensing. In most cases, the policy continues to consume raw RGB observations, where nuisance appearance factors dominate the input distribution [2], [11], [12], [13].

In this work, we instead revisit the *observation interface*. Rather than modifying the policy architecture or scaling data, we explicitly control what the policy sees. We leverage promptable segmentation foundation models [14], [15] to construct a task-aware visual abstraction that suppresses appearance variation while preserving action-relevant structure.

¹Authors are at Mohamed bin Zayed University of Artificial Intelligence (MBZUAI), Abu Dhabi, UAE. Email: {firstname.lastname}@mbzuai.ac.ae

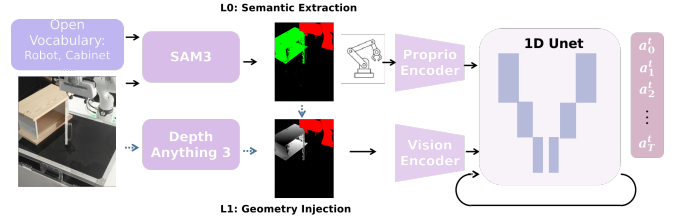


Fig. 1: **Overview of our observation interface:** Given an RGB frame and open-vocabulary text prompts (*robot/gripper*, *target object*), we construct two observation variants. **L0** uses SAM3 masks to render a canonical label-colored image (constant background; fixed colors for robot/gripper and target). **L1** optionally injects geometry by overwriting the masked regions with normalized monocular depth (Depth Anything 3). Both outputs remain standard 3-channel, image-like inputs for off-the-shelf vision encoders. In our main experiments, we pair the interface with an FMP backbone (1D U-Net unchanged), without modifying the policy architecture.

Concretely, we introduce a two-level observation design. **L0 (Seg-repaint)** segments task-relevant entities (target object and robot/gripper) and repaints the scene into a canonical label-colored image with a constant background. **L1 (Seg+Depth)** further injects masked monocular depth to retain geometric cues when finer spatial structure is important. Both representations remain standard 3-channel, image-like inputs and can be paired with existing policy backbones without architectural modification.

We evaluate the proposed interface under controlled appearance shifts on RoboMimic, ManiSkill, and RL Bench, as well as on a real Franka robot. Across both flow-matching and VLA-style policies, our method preserves in-distribution performance while substantially improving robustness under out-of-distribution visual changes.

Contributions: (1) A task-aware semantic–geometric observation interface that canonicalizes appearance via segmentation-based repainting with optional depth injection, while keeping a standard image input; (2) A systematic robustness evaluation under controlled appearance shifts across simulation and real-world benchmarks, demonstrating consistent OOD gains without additional policy fine-tuning.

II. RELATED WORK

In this section, we review recent progress in (i) visuomotor policy learning, with an emphasis on common visual observation setups and action parameterizations, (ii) modern foundation models for segmentation, and how segmentation/semantic priors are integrated into robot policies to improve robustness and generalization.

A. Visuomotor Policy Learning

Recent visuomotor policies are often built by choosing (i) an observation-conditioning interface—what sensory and task signals the policy conditions on (e.g., multi-view RGB/RGB-D, proprioception, language, or goal images) [16], [17], [18], [19]—and (ii) an action parameterization. Actions are either decoded directly (continuous end-effector deltas or discretized symbols) [10], [3] or generated via implicit refinement, where the network predicts an auxiliary quantity (e.g., diffusion denoiser/score or a flow-matching velocity field) and iterative refinement yields action chunks [1], [6], [7]. Consistent with this view, VLA systems mainly differ in the decoder attached to a VLM backbone: token autoregression [3], [8], [9], continuous regression heads [10], or diffusion/flow-based decoders for continuous action chunks [20], [21], [22].

Across simulation benchmarks, the prevailing camera setup uses one or more third-person RGB views and, when available, an eye-in-hand/wrist view; depth is optional and benchmark-dependent [12], [13]. When wrist observations are unavailable, recent work explores “virtual cameras” that synthesize in-hand views from external observations at test time [23]. Large-scale real-robot datasets further reinforce this multi-view pattern: Open X-Embodiment aggregates multi-robot trajectories at scale [11], and models such as Octo and OpenVLA are trained on this corpus with third-person and optional wrist observations [2], [9].

B. Modern Segmentation Models in Robot Learning

Modern segmentation has shifted toward foundation models that make masks promptable and transferable. Segment Anything (SAM) introduced scalable interactive segmentation [24]; SAM 2 extends it to images and video via memory-based tracking [14]. More recently, SAM 3 targets open-vocabulary “concept” segmentation [15], and SAM 3D extends beyond 2D masks toward 3D-aware reconstruction from images [25]. These advances enable segmentation to serve as a controllable perception interface for policy learning rather than a standalone vision output.

In robotics, segmentation is increasingly used to improve robustness and generalization: Shadow leverages masks for cross-embodiment transfer [26], and object-centric grounding can reduce clutter sensitivity in VLA systems [27]. ARRO similarly applies segmentation/grounding to filter task-irrelevant regions online, improving robustness under visual appearance shifts [28]. Category-level generalization is explored by S2-Diffusion [29] and minimal intermediate representations in PEEK [30], while diffusion-based semantic augmentation scales robustness through synthetic variation [31] and ImitDiff transfers foundation-model priors to distraction-robust policies [32]. Beyond using masks as inputs, recent systems integrate promptable segmentation into policy architectures (e.g., SAM2Act and SAM2Grasp) [33], [34]. Complementary directions study segmentation under adverse sensing (cloth grasping in darkness) [35], motion/flow constraints for robust representations (LAOF) [36], depth-conditioned demonstration generation

(DRAW2ACT) [37]. However, prior work has not provided a controlled, multi-benchmark study of observation-level canonicalization for appearance-shift robustness in visuomotor policies; we propose a segmentation-driven semantic-geometric interface and evaluate it under controlled background and object-appearance shifts.

III. METHODOLOGY

As shown in Fig. 1, we construct a semantic-geometric observation interface using open-vocabulary segmentation and optional depth cues, and train a visuomotor policy on the resulting canonical observations.

A. Problem Setup

We study visuomotor policy learning from demonstrations. At each time step t , the robot observes an RGB image $I_t \in \mathbb{R}^{H \times W \times 3}$ and executes an action $a_t \in \mathbb{R}^{d_a}$. Each episode yields a trajectory $\tau = \{(I_t, a_t)\}_{t=1}^T$, and we are given a dataset of expert demonstrations $\mathcal{D} = \{\tau^{(i)}\}_{i=1}^N$.

Our key design choice is to replace raw RGB with a task-aware extracted observation

$$\tilde{o}_t = g(I_t, c), \quad (1)$$

where c is an open-vocabulary task specification (e.g., an object name), and $g(\cdot)$ suppresses task-irrelevant appearance while preserving action-relevant structure. We instantiate π_θ with a Flow Matching Policy (FMP) [38], [39], while the observation extraction $g(\cdot)$ is policy-agnostic and can be paired with other imitation learning backbones.

Algorithm 1 summarizes the overall pipeline: at each time step we (i) use SAM3 with text prompts to segment the robot/gripper and task object(s), (ii) render a canonical label-colored observation by repainting the image based on the resulting masks (L0), and (iii) optionally inject geometric structure by overwriting the segmented regions with normalized monocular depth (L1). In the following subsections, we detail the construction of L0 and L1 and then describe policy learning with FMP on the resulting observations.

B. Task-Aware Observation Extraction (L0)

Given a raw RGB observation $I_t \in \mathbb{R}^{H \times W \times 3}$, we construct a task-aware observation that *canonicalizes* appearance by rendering the scene into a label-colored canvas. We assume an open-vocabulary task specification c and form text prompts p_t using a fixed template per benchmark (e.g., robot gripper and the target object name). We apply SAM3 with these prompts to obtain binary masks for the robot/gripper and the target object:

$$\begin{aligned} M_t^r &= \text{SAM3}(I_t, p^r), \\ M_t^o &= \text{SAM3}(I_t, p^o), \end{aligned} \quad M_t^r, M_t^o \in \{0, 1\}^{H \times W}. \quad (2)$$

When multiple instances are predicted for a prompt, we take their union. We denote the union mask as $M_t = M_t^r \vee M_t^o$. We then render a canonical, 3-channel label-colored

Algorithm 1 Semantic–Geometric Observation Interface with Two-Level Observations (L0/L1)

Require: Demonstrations $\mathcal{D} = \{\tau^{(i)}\}_{i=1}^N$, task spec c , SAM3, Depth Anything 3 (optional), Canonical colors $\{\kappa_{\text{bg}}, \kappa_{\text{rob}}, \kappa_{\text{obj}}\}$

Ensure: Extracted observations \tilde{o}_t for policy learning and inference

- 1: **for all** trajectory $\tau = \{(I_t, a_t)\}_{t=1}^T$ in \mathcal{D} **do**
- 2: **for** $t = 1$ to T **do**
- 3: Form text prompts p_t from c (e.g., robot gripper, target name)
- 4: $M_t^{\text{rob}} \leftarrow \text{SAM3}(I_t, \text{robot gripper})$
- 5: $M_t^{\text{obj}} \leftarrow \text{SAM3}(I_t, \text{target object})$
- 6: $M_t^{\text{bg}} \leftarrow 1 - \min(1, M_t^{\text{rob}} + M_t^{\text{obj}})$
- 7: $I_t^{\text{ts}} \leftarrow \kappa_{\text{bg}} \cdot \text{broadcast}(M_t^{\text{bg}}) + \kappa_{\text{rob}} \cdot \text{broadcast}(M_t^{\text{rob}}) + \kappa_{\text{obj}} \cdot \text{broadcast}(M_t^{\text{obj}}) \triangleright$ L0: canonical label-colored rendering
- 8: **if** geometry cue enabled **then**
- 9: $\hat{D}_t \leftarrow \text{DepthAnything}(I_t)$
- 10: Normalize \hat{D}_t over $\Omega_t^{\text{obj}} = \{(u, v) \mid M_t^{\text{obj}}(u, v) = 1\}$ to get D_t^{norm}
- 11: $I_t^{\text{dep}} \leftarrow \text{tile}(D_t^{\text{norm}}, 3)$
- 12: $\tilde{o}_t \leftarrow I_t^{\text{ts}} \odot (1 - \text{broadcast}(M_t^{\text{obj}})) + I_t^{\text{dep}} \odot \text{broadcast}(M_t^{\text{obj}}) \triangleright$ L1: overwrite object region
- 13: **else**
- 14: $\tilde{o}_t \leftarrow I_t^{\text{ts}}$
- 15: **end if**
- 16: **end for**
- 17: **end for**

Train: learn π_θ from $\{(\tilde{o}_t, a_t)\}$ using Eq. (7).

Inference: compute \tilde{o}_t as above and condition the policy on \tilde{o}_t .

image by assigning fixed colors to each entity and a constant color to the background:

$$I_t^{\text{L0}} = \kappa \cdot \left(1 - \text{broadcast}(M_t)\right) + \mathbf{c}_r \odot \text{broadcast}(M_t^r) + \mathbf{c}_o \odot \text{broadcast}(M_t^o), \quad (3)$$

where κ is a constant background color (we use $\kappa = \mathbf{0}$), \mathbf{c}_r and \mathbf{c}_o are fixed RGB colors for the robot/gripper and target object, respectively, and $\text{broadcast}(\cdot)$ expands a 2D mask to three channels.

This L0 observation removes most nuisance appearance variation (e.g., textures and colors) while preserving the spatial layout of action-relevant entities.

C. Geometry Injection via Depth Anything (L1)

While L0 suppresses nuisance appearance by mapping the scene to a canonical, entity-colored canvas, some tasks still require geometric cues such as shape and fine spatial structure. We therefore construct L1 by estimating monocular depth with Depth Anything 3 [40] and injecting *masked, normalized* depth into the target-object region, yielding a single 3-channel, image-like observation (no channel concatenation).

a) Monocular depth estimation: Given the raw RGB frame, we predict a dense depth map

$$\hat{D}_t = \text{DepthAnything}(I_t), \quad \hat{D}_t \in \mathbb{R}^{H \times W}. \quad (4)$$

Since monocular depth is scale-ambiguous, we use relative depth normalized within the *target-object* mask M_t^o .

b) Masked depth normalization: Let $\Omega_t^o = \{(u, v) \mid M_t^o(u, v) = 1\}$ denote target-object pixels. We compute

$$D_t^{\text{norm}}(u, v) = \frac{\hat{D}_t(u, v) - d_{\min}}{d_{\max} - d_{\min} + \epsilon}, \quad (u, v) \in \Omega_t^o, \quad (5)$$

where $d_{\min} = \min_{(u, v) \in \Omega_t^o} \hat{D}_t(u, v)$ and $d_{\max} = \max_{(u, v) \in \Omega_t^o} \hat{D}_t(u, v)$. We set $D_t^{\text{norm}}(u, v) = 0$ for $(u, v) \notin \Omega_t^o$.

c) Depth overwrite fusion: We tile the normalized depth map to three channels, $I_t^{\text{dep}} = \text{tile}(D_t^{\text{norm}}, 3)$, and overwrite only the target-object region on the L0 canvas:

$$I_t^{\text{L1}} = I_t^{\text{L0}} \odot (1 - \text{broadcast}(M_t^o)) + I_t^{\text{dep}} \odot \text{broadcast}(M_t^o). \quad (6)$$

The resulting observation remains a 3-channel image that can be processed by standard vision encoders without modifying the policy architecture.

D. Policy Learning with Flow Matching

We instantiate π_θ as a Flow Matching Policy (FMP) [38], [39]. Given the extracted observation \tilde{o}_t (L0/L1), FMP learns a time-dependent vector field $v_\theta(x, s; \tilde{o}_t)$ that transports samples from a simple base distribution to the expert action distribution conditioned on \tilde{o}_t . Training minimizes the flow-matching objective:

$$\mathcal{L}_{\text{FM}}(\theta) = \mathbb{E}_{(\tilde{o}_t, a_t) \sim \mathcal{D}, x_0 \sim p_0, s \sim \mathcal{U}(0, 1)} \left[\|v_\theta(x_s, s; \tilde{o}_t) - \dot{x}_s\|_2^2 \right], \quad (7)$$

where $x_0 \sim p_0$ (e.g., Gaussian distribution), x_s lies on a smooth flow from x_0 to the expert action a_t , and \dot{x}_s is the corresponding target velocity. At inference, we integrate the learned vector field from $s = 0$ to 1 with a lightweight ODE solver to obtain an action sample conditioned on \tilde{o}_t .

IV. EXPERIMENTS

We evaluate whether our task-aware semantic–geometric observation interface improves robustness to appearance shifts—novel object textures/colors and background changes—while preserving in-distribution performance. To isolate the effect of the observation, we keep the policy training pipeline fixed (same backbone, vision encoder, and optimization settings) and vary only the input representation. We report results on two complementary policy families: a flow-matching policy and a vision–language–action model (SmolVLA [41]), demonstrating that the proposed abstraction transfers across backbones rather than being tailored to a single policy.

A. Experimental Setup and Evaluation Protocol

a) Benchmarks and tasks: We conduct experiments on RoboMimic (Lift) [12], ManiSkill (YCB object grasp) [42], and RL Bench (CloseGrill, ToiletSeatDown, CloseMicrowave and OpenBox) [13]. We further validate on real Franka robot arm setup, described in Sec. IV-D.

b) Methods compared: We compare three observation variants: (i) **ORG**: raw images; (ii) **L0**: SAM3-driven canonical label-colored rendering (constant background with fixed colors for robot/gripper and target object; Sec. III-B); and (iii) **L1**: L0 with optional geometry injection by overwriting masked regions with normalized monocular depth from Depth Anything 3 (DA3) (Sec. III-C). All variants share the same policy backbone and training recipe (FMP or SmolVLA); only the input observation is changed.

TABLE I: **RoboMimic Lift: robustness under object and background appearance shifts.** Success rate (%). OOD-Obj denotes cube recoloring; OOD-Bg denotes tabletop color shifts. All results are averaged over 3 seeds (50 rollouts per seed). Mean averages OOD1–3.

Setting	ID	OOD-Obj (Cube Color)				OOD-Bg (Table Color)			
		OOD1	OOD2	OOD3	Mean	OOD1	OOD2	OOD3	Mean
Org (RGB)	98.7	24.0	83.3	81.3	62.0	8.0	46.0	1.3	18.4
L0 (Seg-repaint)	98.7	92.0	89.3	87.3	89.6	90.0	94.7	87.3	90.7
L1 (Seg+Depth)	98.7	92.0	88.7	88.7	89.8	89.3	95.3	88.7	91.1

c) *Appearance-shift (OOD) protocol:* We report both in-distribution (ID) and out-of-distribution (OOD) performance. ID uses the standard benchmark visual settings. For OOD, we introduce controlled appearance shifts that are *held out* from training:

- **OOD-Obj:** novel object appearances via unseen colors.
- **OOD-Bg:** novel scene appearance via background color changes and/or additional clutter distractors.

We keep task success definitions unchanged, isolating appearance as the primary source of distribution shift.

d) *Implementation details:* We train each method with the same network architecture, optimizer, and training epochs and report mean over 3 random seeds. For our observation extractor, SAM3 is prompted by the open-vocabulary task specification (text prompt) (Sec. III-B). Depth is estimated from RGB using DA3 and normalized within the segmented region before overwrite fusion (Sec. III-C). SAM3/DA3 are adapted on the ID training split only; no OOD data is used for perception adaptation.

B. Foundation Models Adaptation and Usage

We adapt the foundation models used by our observation interface (SAM3 for segmentation and DA3 for monocular depth) with lightweight LoRA adapters [43] to match the visual statistics of each benchmark. Importantly, we fine-tune these models using only the in-distribution (ID) training data used to train the policy, and do not use any OOD data for perception adaptation.

a) *SAM3 LoRA fine-tuning:* To improve segmentation reliability, we fine-tune SAM3 using LoRA adapters. Each RGB frame yields two training samples: (i) a robot/gripper union mask and (ii) a task-object union mask, paired with fixed text prompts (e.g., *robot gripper, target object*). We freeze the SAM3 backbone and insert LoRA modules into the *text encoder* self-attention projections, targeting *q_proj* and *v_proj* in the *last 4* transformer blocks. We use LoRA rank $r=8$, $\alpha=16$, dropout 0.05, and train for 50 epochs with AdamW (lr 5×10^{-4} , weight decay 10^{-2}) under mixed precision. We optimize a standard mask supervision loss, $\mathcal{L} = \mathcal{L}_{\text{BCE}} + 0.5 \mathcal{L}_{\text{Dice}}$, computed between the predicted mask logits and ground-truth masks. The same LoRA-adapted SAM3 checkpoint is used for all runs within a benchmark and applied at test time without further adaptation.

b) *DA3 LoRA fine-tuning:* To better preserve task-relevant geometry under appearance variation, we adapt Depth Anything 3 (DA3) with lightweight LoRA while keeping the pretrained backbone frozen. Specifically, we

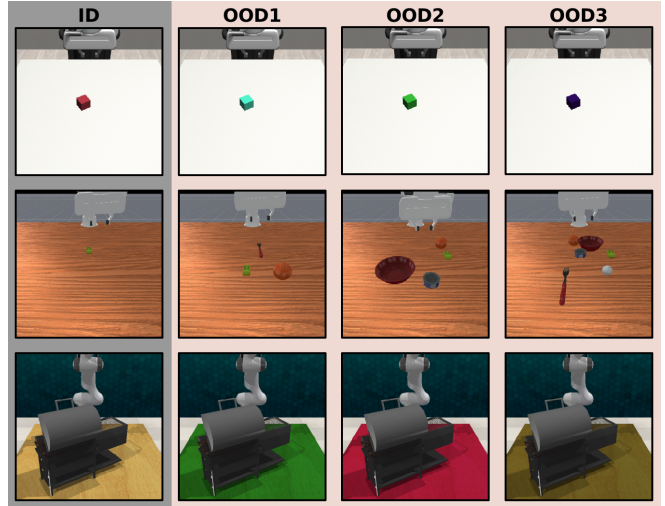


Fig. 2: **Evaluation environments under controlled appearance shifts.** Each row shows the in-distribution (ID) training setting and three held-out test variants (OOD1–3), with task dynamics unchanged. **Row 1:** RoboMimic Lift under *object appearance* shifts (OOD-Obj): ID uses the training cube appearance, while OOD1–3 recolor the cube. **Row 2:** ManiSkill YCB grasping under increasing clutter: ID is the uncluttered training scene; OOD1–3 introduce novel distractor object sets/layouts. **Row 3:** RL-Bench tabletop *background* shifts (OOD-Bg): ID uses the training tabletop appearance, while OOD1–3 change the tabletop color.

TABLE II: **ManiSkill: YCB grasping under increasing clutter.** Success rate (%). **ID** denotes the training scene configuration. **OOD1–3** are more challenging test scenes with different YCB object combinations (increased clutter/distractors). **Mean** averages over OOD1–3.

Setting	ID	OOD1	OOD2	OOD3	Mean
Org (RGB)	98.0	25.0	10.0	10.0	15.0
L0 (Seg-repaint)	96.0	96.0	92.0	92.0	93.3
L1 (Seg+Depth)	96.0	96.0	92.0	94.0	94.0

insert LoRA modules into selected `nn.Linear` layers of the DA3 encoder, targeting attention and MLP projection layers (e.g., `qkv/q_proj/k_proj/v_proj/out_proj` and `fc1/fc2`), and optimize only the LoRA parameters. Training uses paired RGB–depth supervision with DA3-style preprocessing: images are resized with an upper-bound strategy to `process_res=504`, aligned to `patch_size=14`, and ImageNet-normalized. We minimize the scale-invariant SILog loss ($\lambda=0.85$). We use LoRA rank $r=8$, $\alpha=16$, dropout 0.05, and AdamW with lr 10^{-4} (weight decay 0) for 100 epochs. (For real-robot experiments, we use the pretrained DA3 model as-is; DA3 LoRA adaptation is only applied in simulation benchmarks.)

C. Simulation Benchmarks

We evaluate robustness to appearance shifts on three simulation benchmarks: RoboMimic, ManiSkill, and RL-Bench. For each benchmark, we report in-distribution (ID) performance under the default visual configuration and out-of-distribution (OOD) performance under controlled appearance changes. All methods use the same policy backbone (FMP) and training budget; only the input observation differs (Sec. IV-A).

TABLE III: **RLBench: robustness under tabletop color shifts.** Success rate (%). For each task, FMPs are evaluated under the training tabletop color (ID) and three held-out tabletop colors (OOD1–3). Each entry is averaged over 50 rollouts per seed and 3 random seeds.

Obs.	CloseGrill				ToiletSeatDown				CloseMicrowave				OpenBox			
	ID	OOD1	OOD2	OOD3	ID	OOD1	OOD2	OOD3	ID	OOD1	OOD2	OOD3	ID	OOD1	OOD2	OOD3
Org (RGB)	84.0	14.7	30.7	48.0	94.7	14.7	47.3	52.7	80.7	7.3	11.3	10.7	60.0	1.3	1.3	4.7
L0 (Seg-repaint)	74.7	73.3	74.0	73.3	83.3	83.3	80.7	80.7	86.7	84.7	82.7	83.3	60.0	52.0	54.7	52.0
L1 (Seg+Depth)	82.7	81.3	82.0	82.0	91.3	89.3	89.3	87.3	96.7	92.0	91.3	89.3	62.0	62.0	57.3	51.3

a) *RoboMimic (Lift): object & support-surface color shifts:* On RoboMimic Lift, we test robustness to changes in the cube appearance (OOD-Obj) and the table/support-surface appearance (OOD-Bg). OOD-Obj varies the cube color relative to training, while OOD-Bg changes the dominant tabletop color without altering task dynamics. Tab. I summarizes the results.

Under both cube-color and tabletop-color shifts, raw RGB exhibits severe brittleness: the mean success drops from 98.7% (ID) to 62.0% under OOD-Obj and further to 18.4% under OOD-Bg (Tab. I), with some tabletop colors nearly collapsing performance (e.g., 1.3% on OOD3). In contrast, segmentation-based repainting (L0) substantially stabilizes performance across appearances, improving mean OOD success to 89.6% (OOD-Obj) and 90.7% (OOD-Bg).

Adding depth-guided geometry preservation (L1) yields only marginal changes on Lift: L1 is comparable to L0 for OOD-Obj (89.8% vs. 89.6% mean) and OOD-Bg (91.1% vs. 90.7% mean), without a consistent advantage across individual OOD settings. This is expected because Lift is largely governed by coarse object localization and reaching, where segmentation already removes most nuisance appearance and the remaining geometric ambiguity is limited; consequently, explicit depth cues provide little additional benefit beyond semantic filtering in this task.

b) *ManiSkill (YCB Object grasp): unclutter-to-clutter generalization:* We study a YCB-style grasping task (green lego). Policies are trained in a non-cluttered environment (ID) and evaluated in visually distinct cluttered environments (OOD-Bg) containing distractor objects and different scene layouts. This isolates robustness to background clutter and distractors. Tab. II reports success rates under increasing clutter.

The raw RGB baseline is highly sensitive to clutter: although it achieves 98.0% success in ID, performance drops sharply in cluttered scenes (OOD mean 15.0%), indicating that distractors and background complexity substantially disrupt visuomotor inference. In contrast, both segmentation-based observation variants are robust across clutter levels. L0 (Seg-repaint) maintains high success under OOD (mean 93.3%), demonstrating that suppressing task-irrelevant regions is sufficient to recover most of the lost performance. Adding depth-guided geometry preservation (L1) provides only a small additional gain over L0 in this grasping setup (OOD mean 94.0% vs. 93.3%), suggesting that once the target is isolated from distractors, monocular-depth cues offer limited incremental benefit for this relatively local grasping task.

TABLE IV: **Real robot: robustness under background/support-surface appearance shifts.** Success rate (%). Each ID/OOD setting is evaluated with 20 rollouts per seed and averaged over 3 training seeds. ID denotes the training appearance; OOD1–2 are held-out support-surface/background configurations. For ReachX we use L0; for CloseCabinet we use L1.

Obs.	ReachX			CloseCabinet		
	ID	OOD1	OOD2	ID	OOD1	OOD2
Org (RGB)	61.7	21.7	25.0	85.0	45.0	48.3
L0 / L1	88.3	83.3	81.7	81.7	78.3	75.0

c) *RLBench: tabletop color shifts:* We evaluate on RLBench tasks CloseGrill, ToiletSeatDown, CloseMicrowave, and OpenBox. ID uses the default training appearance, while OOD-Bg changes the dominant tabletop color (OOD1–3) without altering task dynamics. Table III summarizes success rates under these controlled background shifts.

Across all four tasks, the raw-RGB baseline degrades sharply under OOD-Bg: for example, CloseMicrowave drops from 80.7% (ID) to 7.3–11.3% (OOD), and OpenBox drops from 60.0% (ID) to near-zero success (1.3–4.7%). In contrast, segmentation-based repainting (L0) substantially stabilizes performance under background changes, recovering strong OOD success on CloseGrill (73.3–74.0%), ToiletSeatDown (80.7–83.3%), and CloseMicrowave (82.7–86.7%), and improving OpenBox to 52.0–54.7%.

Adding the geometry cue (L1) further improves or maintains robustness, with the clearest gains on CloseMicrowave (ID 80.7% \rightarrow 96.7%; OOD 89.3–92.0%) and moderate improvements on CloseGrill and ToiletSeatDown. For OpenBox, L1 helps in one OOD setting (OOD1 62.0%) but is not uniformly better than L0 (e.g., OOD3 51.3% vs. 52.0%), suggesting the depth-guided overwrite is most beneficial on tasks where finer spatial structure is the limiting factor rather than distractor suppression alone.

D. Real Robot Experiments

We further validate the proposed observation interface on a real Franka robot under controlled appearance shifts (Fig. 3). We consider two manipulation tasks.

a) *Task 1: ReachX:* The robot moves the end-effector to touch the marker labeled “X” among three planar markers. Marker layout and support-surface appearance vary across ID and OOD settings. As this task primarily requires planar localization, we compare Org (RGB) and L0.

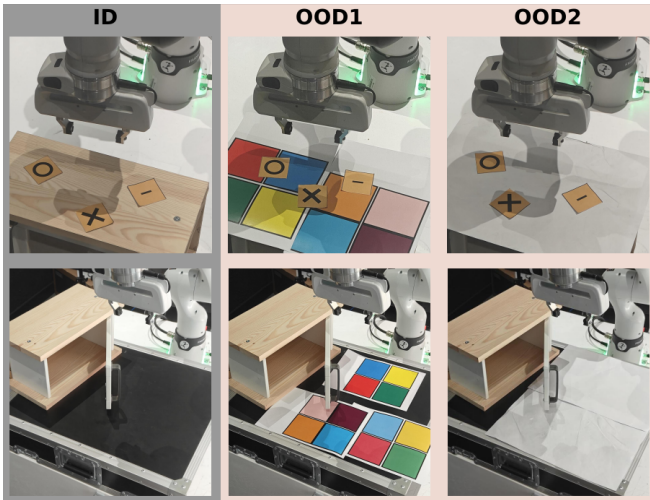


Fig. 3: **Real-robot evaluation scenes under controlled appearance shifts.** We evaluate two tasks on a Franka arm under one in-distribution condition (**ID**) and two held-out support-surface/background appearances (**OOD1–2**). **Top row:** ReachX (reaching to a target marker). **Bottom row:** CloseCabinet (closing the cabinet). Across columns, task setup and camera viewpoint are kept fixed; only the visual appearance of the support surface/background is changed.

b) Task 2: CloseCabinet: The robot closes a partially open cabinet. This task requires contact and spatial alignment; accordingly, we compare Org (RGB) and L1.

c) Deployment protocol: We deploy the Flow Matching Policy (FMP) to predict a target joint state conditioned on the extracted observation (L0 or L1) from the current and previous frames. The predicted state is executed via franky control library [44], which tracks the target using low-level joint control. No additional policy fine-tuning or test-time adaptation is performed under OOD appearances.

For each task, we collect 25 demonstrations using GELLO [45]. In each run, 20 demonstrations are used for training and 5 are held out; training is repeated with three random splits.

For L0, segmentation masks used to construct the training set are obtained using SAM3 with text prompts; when text prompting fails, a minimal click prompt is provided to correct the mask, and the resulting masks are used to fine-tune SAM3 via LoRA on the training data only. At inference time, segmentation relies solely on text prompts.

For L1, monocular depth is estimated using the pretrained Depth Anything 3 model without fine-tuning on real-robot data. No OOD data is used for perception adaptation, and both perception models remain fixed during policy training and evaluation.

At test time, we evaluate 20 rollouts per trained model under each ID/OOD condition, varying object/cabinet pose and support-surface appearance. Success rates averaged over three seeds are reported in Table IV. On an RTX 4060 Ti, SAM3 takes ≈ 0.015 s per prompt (robot+object ≈ 0.03 s/frame), and Depth Anything 3 takes ≈ 0.052 s/frame. This latency is compatible with our target-joint tracking setup and task dynamics, which do not demand high-frequency

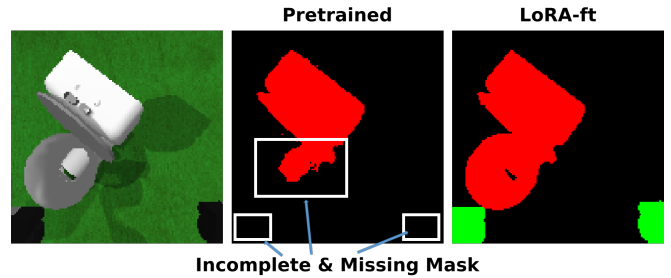


Fig. 4: **Qualitative comparison of SAM3 segmentation before/after LoRA fine-tuning.** Left: wrist-camera RGB observation from an OOD tabletop-color setting (see Fig. 2). Middle: pretrained SAM3 often misses parts of the robot/gripper and produces incomplete masks. Right: our LoRA-finetuned SAM3 produces accurate robot/gripper and object masks under the same OOD setting.

visual updates.

d) Results: On ReachX, the RGB baseline drops from 61.7% (ID) to 21.7% / 25.0% (OOD1/2). In contrast, L0 maintains strong performance across conditions (88.3% ID; 83.3% / 81.7% OOD), substantially reducing the robustness gap.

On CloseCabinet, RGB degrades from 85.0% (ID) to 45.0% / 48.3% (OOD1/2), whereas L1 improves OOD robustness to 78.3% / 75.0% while maintaining comparable ID performance (81.7%). These results are consistent with simulation: L0 performs well on marker reaching, and L1 maintains robust performance on the cabinet-closing task under appearance shifts.

E. Ablations

a) Robot/gripper mask ablation: Beyond segmenting the task-relevant object, we examine whether explicitly including the robot/gripper in the SAM3 vocabulary is necessary. As shown in Table V, retaining only the target object (Target-only) causes performance to collapse on both RoboMimic Lift (7.3%) and RL Bench CloseGrill (5.3%). This suggests that masking out the robot removes action-critical visual state—e.g., gripper pose, approach direction, and contact configuration—which is essential for mapping observations to actions. In contrast, adding the robot/gripper mask (Target+Robot) restores strong performance (98.7% on Lift, 74.7% on CloseGrill), indicating that the robot itself should be treated as a first-class entity in the task-aware observation interface.

TABLE V: Robot/gripper mask ablation. Success rate (%) for FMP when the SAM3 mask vocabulary includes the robot/gripper in addition to the target object. Mean over 3 seeds (50 rollouts/seed).

Task	Target-only	Target+Robot
RoboMimic Lift	7.3	98.7
RLBench CloseGrill	5.3	74.7

b) SAM3 fine-tuning ablation: We evaluate the impact of LoRA fine-tuning on SAM3 segmentation quality under ID and held-out tabletop appearances. Table VI reports mask IoU on ToiletSeatDown for the robot/gripper (R-IoU) and the target object (O-IoU).

TABLE VI: **SAM3 segmentation quality (IoU) before/after fine-tuning on ToiletSeatDown**. IoU (%) on **robot/gripper** (R-IoU) and **target object** (O-IoU) masks under the in-distribution setting (ID) and two held-out tabletop colors (OOD1–2).

Model	R-IoU (%)			O-IoU (%)		
	ID	OOD1	OOD2	ID	OOD1	OOD2
Pretrained	0.0	0.0	0.0	23.9	32.9	14.0
LoRA-ft	99.3	98.9	99.1	99.5	99.2	99.2

TABLE VII: **RLBench: SmolVLA robustness under tabletop color shifts**. Success rate (%) on `CloseGrill` and `CloseMicrowave` using three observation variants. ID denotes the training tabletop color; OOD1/2 correspond to the held-out *green* and *red* tabletop colors, respectively.

Obs.	CloseGrill			CloseMicrowave		
	ID	OOD1	OOD2	ID	OOD1	OOD2
Org (RGB)	76.0	46.0	42.0	64.0	4.0	8.0
L0 (Seg-repaint)	70.0	64.0	66.0	70.0	64.0	60.0
L1 (Seg+Depth)	72.0	66.0	66.0	84.0	78.0	76.0

The pretrained SAM3 fails to recover the robot/gripper mask (0.0% R-IoU) and yields low-quality object masks (14.0–32.9% O-IoU). LoRA fine-tuning substantially improves segmentation, achieving 98.9–99.3% R-IoU and 99.2–99.5% O-IoU consistently across ID and OOD settings. Figure 4 shows an OOD example: the pretrained model misses the gripper and produces incomplete object masks, while the LoRA-finetuned model segments both reliably.

c) Generalization to VLA backbones (SmolVLA): To verify that our observation interface is *policy-agnostic* and not tailored to Flow Matching Policy (FMP), we additionally fine-tune and evaluate a representative vision–language–action model, SmolVLA [41], on RLBench. Table VII reports success rates under the training tabletop appearance (ID) and two held-out tabletop colors (OOD1/2). While raw RGB already attains reasonable ID performance, it degrades substantially under appearance shifts—most notably on `CloseMicrowave`, where success drops from 64.0% (ID) to 4.0%/8.0% (OOD1/2). In contrast, our semantic repainting (L0) markedly improves robustness on both tasks, increasing OOD success to 64.0%/60.0% on `CloseMicrowave` and 64.0%/66.0% on `CloseGrill`. Injecting depth geometry (L1) further boosts performance on the more geometry-sensitive `CloseMicrowave`, improving both ID (84.0%) and OOD (78.0%/76.0%) while maintaining strong robustness on `CloseGrill`. These results indicate that the proposed observation mapping consistently stabilizes policy rollouts across visual shifts beyond diffusion/flow-style policies, and transfers to VLA-style controllers without any backbone-specific modification.

d) Compare with S2Diffusion: S2Diffusion [29] is closely related to our setting: it combines segmentation and monocular depth cues by channel-wise concatenation to form a spatial–semantic observation. Since the paper does not specify how this multi-channel tensor is fed into a standard 3-channel ResNet encoder, we implement an S2-style baseline in our FMP framework by constructing a 2-channel input with channel-0 = binary mask and channel-1 = normalized depth (matching our dataset), and adding

TABLE VIII: **S2Diffusion-style observation encoding vs. our L1**. Success rate (%) averaged over 3 seeds (50 rollouts/seed). S2-style uses a 2-channel input (mask, depth) with a 1×1 conv adapter (2→3) before the same 3-channel ResNet encoder; all other FMP settings are identical.

Task	Method	ID	OOD1	OOD2	OOD3
CloseGrill	S2-style	48.7	45.3	40.0	42.7
	Ours (L1)	82.7	81.3	82.0	82.0
CloseMicrowave	S2-style	64.0	60.7	58.7	61.3
	Ours (L1)	96.7	92.0	91.3	89.3

a lightweight 1×1 conv adapter (2→3) before the visual encoder to avoid modifying the ResNet backbone. As shown in Table VIII, this S2-style representation underperforms our L1 repaint/overwrite observation on both `CloseGrill` and `CloseMicrowave`, in-distribution and under background shifts (OOD1–3).

V. CONCLUSION

We presented a task-aware semantic–geometric observation interface that leverages vision foundation models for segmentation and monocular depth to canonicalize visual input via segmentation-based repainting (L0) and optional depth injection (L1), improving robustness to appearance shifts without modifying the policy backbone.

Across RoboMimic, ManiSkill, and RLBench, the proposed interface preserves in-distribution performance while substantially improving robustness under object and background appearance changes. The same abstraction benefits both Flow Matching Policies and SmolVLA, indicating backbone-agnostic gains. Real-robot experiments on a Franka arm further confirm that the interface significantly reduces performance degradation under support-surface shifts without additional policy fine-tuning or test-time adaptation.

These results highlight the importance of revisiting the observation interface as a complementary approach to scaling policy capacity for robust visuomotor learning.

REFERENCES

- [1] C. Chi, Z. Xu, S. Feng, E. Cousineau, Y. Du, B. Burchfiel, R. Tedrake, and S. Song, “Diffusion policy: Visuomotor policy learning via action diffusion,” *The International Journal of Robotics Research*, vol. 44, no. 10-11, pp. 1684–1704, 2025.
- [2] O. M. Team, D. Ghosh, H. Walke, K. Pertsch, K. Black, O. Mees, S. Dasari, J. Hejna, T. Kreiman, C. Xu *et al.*, “Octo: An open-source generalist robot policy,” in *Proceedings of Robotics: Science and Systems*, 2024.
- [3] A. Brohan, N. Brown, J. Carbajal, Y. Chebotar, J. Dabis, C. Finn, K. Gopalakrishnan, K. Hausman, A. Herzog, J. Hsu *et al.*, “Rt-1: Robotics transformer for real-world control at scale,” in *Proceedings of Robotics: Science and Systems*, 2023.
- [4] R. Garcia, R. Strudel, S. Chen, E. Arlaud, I. Laptev, and C. Schmid, “Robust visual sim-to-real transfer for robotic manipulation,” in *2023 IEEE/RSJ International Conference on Intelligent Robots and Systems (IROS)*. IEEE, 2023, pp. 992–999.
- [5] P. Wilbert, S. Ishika, D. Jiafei, K. Ranjay, T. Jesse, and F. Dieter, “THE COLOSSEUM: A Benchmark for Evaluating Generalization for Robotic Manipulation,” in *Proceedings of Robotics: Science and Systems*, 2024.
- [6] H. Ding, N. Jaquier, J. Peters, and L. Rozo, “Fast and robust visuomotor riemannian flow matching policy,” *IEEE Transactions on robotics*, 2025.

- [7] Q. Zhang, Z. Liu, H. Fan, G. Liu, B. Zeng, and S. Liu, "Flowpolicy: Enabling fast and robust 3d flow-based policy via consistency flow matching for robot manipulation," in *Proceedings of the AAAI Conference on Artificial Intelligence*, vol. 39, no. 14, 2025, pp. 14754–14762.
- [8] B. Zitkovich, T. Yu, S. Xu, P. Xu, T. Xiao, F. Xia, J. Wu, P. Wohlhart, S. Welker, A. Wahid *et al.*, "Rt-2: Vision-language-action models transfer web knowledge to robotic control," in *Conference on Robot Learning*. PMLR, 2023, pp. 2165–2183.
- [9] M. J. Kim, K. Pertsch, S. Karamcheti, T. Xiao, A. Balakrishna, S. Nair, R. Rafailov, E. P. Foster, P. R. Sanketi, Q. Vuong, T. Kollar, B. Burchfiel, R. Tedrake, D. Sadigh, S. Levine, P. Liang, and C. Finn, "OpenVLA: An open-source vision-language-action model," in *8th Annual Conference on Robot Learning*, 2024.
- [10] X. Li, M. Liu, H. Zhang, C. Yu, J. Xu, H. Wu, C. Cheang, Y. Jing, W. Zhang, H. Liu, H. Li, and T. Kong, "Vision-language foundation models as effective robot imitators," in *The Twelfth International Conference on Learning Representations*, 2024.
- [11] A. O'Neill, A. Rehman, A. Maddukuri, A. Gupta, A. Padalkar, A. Lee, A. Pooley, A. Gupta, A. Mandlekar, A. Jain *et al.*, "Open x-embodiment: Robotic learning datasets and rt-x models: Open x-embodiment collaboration 0," in *2024 IEEE International Conference on Robotics and Automation (ICRA)*. IEEE, 2024, pp. 6892–6903.
- [12] A. Mandlekar, D. Xu, J. Wong, S. Nasiriany, C. Wang, R. Kulkarni, L. Fei-Fei, S. Savarese, Y. Zhu, and R. Martín-Martín, "What matters in learning from offline human demonstrations for robot manipulation," in *Conference on Robot Learning (CoRL)*, 2021.
- [13] S. James, Z. Ma, D. Rovick Arrojo, and A. J. Davison, "Rlbench: The robot learning benchmark & learning environment," *IEEE Robotics and Automation Letters*, 2020.
- [14] N. Ravi, V. Gabeur, Y.-T. Hu, R. Hu *et al.*, "SAM 2: Segment anything in images and videos," in *The Thirteenth International Conference on Learning Representations*, 2025.
- [15] N. Carion, L. Gustafson, Y.-T. Hu, S. Debnath *et al.*, "SAM 3: Segment anything with concepts," in *The Fourteenth International Conference on Learning Representations*, 2026.
- [16] Y. Jiang, A. Gupta, Z. Zhang, G. Wang, Y. Dou, Y. Chen, L. Fei-Fei, A. Anandkumar, Y. Zhu, and L. Fan, "Vima: General robot manipulation with multimodal prompts," in *Fortieth International Conference on Machine Learning*, 2023.
- [17] M. Shridhar, L. Manuelli, and D. Fox, "Perceiver-actor: A multi-task transformer for robotic manipulation," in *Conference on Robot Learning*. PMLR, 2023, pp. 785–799.
- [18] E. Jang, A. Irpan, M. Khansari, D. Kappler, F. Ebert, C. Lynch, S. Levine, and C. Finn, "Bc-z: Zero-shot task generalization with robotic imitation learning," in *Conference on Robot Learning*. PMLR, 2022, pp. 991–1002.
- [19] O. Mees, L. Hermann, E. Rosete-Beas, and W. Burgard, "Calvin: A benchmark for language-conditioned policy learning for long-horizon robot manipulation tasks," *IEEE Robotics and Automation Letters*, vol. 7, no. 3, pp. 7327–7334, 2022.
- [20] P. Intelligence, K. Black, N. Brown, J. Darpinian, K. Dhabalia, D. Driess, A. Esmail, M. Equi, C. Finn, N. Fusai *et al.*, " $\pi_{0.5}$: a vision-language-action model with open-world generalization," in *Proceedings of The 9th Conference on Robot Learning*, 2025, pp. 17–40.
- [21] Q. Li, Y. Liang, Z. Wang, L. Luo, X. Chen, M. Liao, F. Wei, Y. Deng, S. Xu, Y. Zhang *et al.*, "Cogact: A foundational vision-language-action model for synergizing cognition and action in robotic manipulation," *arXiv preprint arXiv:2411.19650*, 2024.
- [22] J. Liu, H. Chen, P. An, Z. Liu, R. Zhang, C. Gu, X. Li, Z. Guo, S. Chen, M. Liu *et al.*, "Hybridvla: Collaborative diffusion and autoregression in a unified vision-language-action model," *arXiv preprint arXiv:2503.10631*, 2025.
- [23] H. Ding, A. Duan, Z. Sun, D. Song, and Y. Nakamura, "Imagination at inference: Synthesizing in-hand views for robust visuomotor policy inference," *arXiv preprint arXiv:2509.15717*, 2025.
- [24] A. Kirillov, E. Mintun, N. Ravi, H. Mao, C. Rolland, L. Gustafson, T. Xiao, S. Whitehead, A. C. Berg, W.-Y. Lo *et al.*, "Segment anything," in *Proceedings of the IEEE/CVF international conference on computer vision*, 2023, pp. 4015–4026.
- [25] X. Chen, F.-J. Chu, P. Gleize, K. J. Liang, A. Sax, H. Tang, W. Wang, M. Guo, T. Hardin, X. Li *et al.*, "Sam 3d: 3dfy anything in images," *arXiv preprint arXiv:2511.16624*, 2025.
- [26] M. Lepert, R. Doshi, and J. Bohg, "Shadow: Leveraging segmentation masks for cross-embodiment policy transfer," in *Conference on Robot Learning*. PMLR, 2025, pp. 3536–3550.
- [27] K. Vo, T. Hanyu, Y. Ikebe, T. T. Pham, N. Chung, M. N. Vu, D. N. H. Minh, A. Nguyen, A. Gunderman, C. Rainwater *et al.*, "Clutter-resistant vision-language-action models through object-centric and geometry grounding," *arXiv preprint arXiv:2512.22519*, 2025.
- [28] R. Mirjalili, T. Jülg, F. Walter, and W. Burgard, "Augmented reality for robots (arro): Pointing visuomotor policies towards visual robustness," *arXiv preprint arXiv:2505.08627*, 2025.
- [29] Q. Yang, M. C. Welle, D. Kragic, and O. Andersson, "S²-diffusion: Generalizing from instance-level to category-level skills in robot manipulation," *IEEE Robotics and Automation Letters*, vol. 10, no. 12, pp. 12995–13002, 2025.
- [30] J. Zhang, M. Memmel, K. Kim, D. Fox, J. Thomason, F. Ramos, E. Biryk, A. Gupta, and A. Li, "Peek: Guiding and minimal image representations for zero-shot generalization of robot manipulation policies," *arXiv preprint arXiv:2509.18282*, 2025.
- [31] T. Yu, T. Xiao, A. Stone, J. Tompson, A. Brohan, S. Wang, J. Singh, C. Tan, J. Peralta, B. Ichter *et al.*, "Scaling robot learning with semantically imagined experience," *Robotics: Science and Systems*, 2019.
- [32] Y. Dong, H. Ge, Y. Zeng, J. Zhang, B. Tian, H. Zhu, Y. Jia, R. Wang, Z. Xue, G. Zhou *et al.*, "Imitdiff: Transferring foundation-model priors for distraction-robust visuomotor policy," *IEEE Robotics and Automation Letters*, 2025.
- [33] H. Fang, M. Grotz, W. Pumacay, Y. R. Wang, D. Fox, R. Krishna, and J. Duan, "SAM2act: Integrating visual foundation model with a memory architecture for robotic manipulation," in *Forty-second International Conference on Machine Learning*, 2025.
- [34] S. Wu, J. Yang, W. Luo, L. Gao, C. Shang, M. Zhi, M. Sun, F. Yang, L. Ren, and Y. Zhao, "Sam2grasp: Resolve multi-modal grasping via prompt-conditioned temporal action prediction," *arXiv preprint arXiv:2512.02609*, 2025.
- [35] X. Zhu, H. Zhong, Y. Wu, S. Luo, and Y. Gao, "Guiding robotic cloth grasping in darkness: Infrared semantic segmentation and grasping position selection," *IEEE Robotics and Automation Letters*, vol. 11, no. 1, pp. 546–553, 2025.
- [36] X. Bu, J. Lyu, F. Sun, R. Yang, Z. Ma, and W. Li, "Laof: Robust latent action learning with optical flow constraints," *arXiv preprint arXiv:2511.16407*, 2025.
- [37] Y. Bai, L. Yang, G. Eskandar, F. Shen, M. Altillawi, Z. Liu, and G. Kutyoniok, "Draw2act: Turning depth-encoded trajectories into robotic demonstration videos," *arXiv preprint arXiv:2512.14217*, 2025.
- [38] M. Braun, N. Jaquier, L. Rozo, and T. Asfour, "Riemannian flow matching policy for robot motion learning," in *2024 IEEE/RSJ International Conference on Intelligent Robots and Systems (IROS)*. IEEE, 2024, pp. 5144–5151.
- [39] Q. Rouxel, A. Ferrari, S. Ivaldi, and J.-B. Mouret, "Flow matching imitation learning for multi-support manipulation," in *2024 IEEE-RAS 23rd International Conference on Humanoid Robots (Humanoids)*. IEEE, 2024, pp. 528–535.
- [40] H. Lin, S. Chen, J. H. Liew, D. Y. Chen, Z. Li, G. Shi, J. Feng, and B. Kang, "Depth anything 3: Recovering the visual space from any views," in *The Fourteenth International Conference on Learning Representations*, 2026.
- [41] M. Shukor, D. Aubakirova, F. Capuano, P. Kooijmans, S. Palma, A. Zouitine, M. Aractingi, C. Pascal, M. Russi, A. Marafioti *et al.*, "Smolvla: A vision-language-action model for affordable and efficient robotics," *arXiv preprint arXiv:2506.01844*, 2025.
- [42] S. Tao, F. Xiang, A. Shukla, Y. Qin, X. Hinrichsen, X. Yuan, C. Bao, X. Lin, Y. Liu *et al.*, "Maniskill3: Gpu parallelized robotics simulation and rendering for generalizable embodied ai," *Robotics: Science and Systems*, 2025.
- [43] S. Mangrulkar, S. Gugger, L. Debut, Y. Belkada, S. Paul, B. Bossan, and M. Tietz, "PEFT: State-of-the-art parameter-efficient fine-tuning methods," <https://github.com/huggingface/peft>, 2022.
- [44] T. Schneider, "Franky: High-level control library for franka robots," 2025. [Online]. Available: <https://github.com/TimSchneider42/franky>
- [45] P. Wu, Y. Shentu, Z. Yi, X. Lin, and P. Abbeel, "Gello: A general, low-cost, and intuitive teleoperation framework for robot manipulators," in *2024 IEEE/RSJ International Conference on Intelligent Robots and Systems (IROS)*, 2024, pp. 12156–12163.